Biomass Conversion and Biorefinery (2024) 14:17329–17339
https://doi.org/10.1007/s13399-023-04120-0

ORIGINAL ARTICLE

Nonmagnetic nanocomposite of strontium, copper, and manganese oxide in rapid degradation of industrial organic dyes under assistance of sunlight

Saikatendu Deb Roy[1,2] · Bireshwar Bhattacharjee[3,4] · Krishna Chandra Das[2] · Siddhartha Sankar Dhar[1]

Received: 11 November 2022 / Revised: 13 March 2023 / Accepted: 21 March 2023 / Published online: 29 March 2023

Abstract

Green synthesis of metal oxide nanoparticles has played a significant role in modernizing technology. In the present work, *Carica papaya* fruit extract has been used to synthesize a mixed metal nano composite of Sr/Cu/MnO via the coprecipitation method. The synthesized material is washed, dried, and calcined at 530 °C. The composite is analyzed using XRD, SEM, TEM, and EDS. The particle sizes are determined from XRD data, and the crystallite strain is calculated using the Willamson–Hall plot. The crystallinity index is calculated from the TEM images. The particles seem to have polycrystalline nature and hexagonal texture with surface agglomeration. The elemental presence is confirmed by EDS data. The nano-oxide mixture in catalytic amount is then used to degrade aniline blue and malachite green without the addition of any acid. Aniline blue is 74.21% degraded and malachite green is 91.07% degraded in 150 min, representing its potential as a photocatalyst. The theoretical calculation on the degradation data reveals the estimated time for 100% degradation of both dyes.

Keywords Nanocomposite · Synthetic strategies · Dye degradation · Willamson–Hall · Linear regression model · Malachite green and aniline blue

Abbreviation

MG Malachite green
AB Aniline blue

1 Introduction

Synthetic dyes have found large-scale use in industries such as textile, leather, food production, and paper industries [1]. Classic blue, orange II, methylene blue, and malachite green are potential dyes used in industries and are primarily used for dyeing cotton silk, paper leather, etc. [1–8]. When released into the water bodies, these dyes affect and pollute the aquatic environment, which has significant impacts on the kidney, liver, gills, and pituitary glands of aquatic organisms [9]. The above mentioned dyes are potential carcinogens and can confer toxicity in plant and animal growth [10, 11]. Many developments in removing such organic pollutants have been made, and advances in auto-oxidation using ozone, titanium dioxide, ultraviolet (UV) [7], and Fenton's reagent have scanned the attention in the removal of organic pollutants treating water quality. The reports suggest that Fenton's reaction is the most effective method for degrading organic pollutants [12–14]. The use of Fe^{2+} in nanocomposite for the treatment of water is already known; here, we try to find an alternative to Fe^{2+} for the degradation of dyes. The major role in degradation is always played by the alteration in the pH of the degradation medium [15–19]. The degradation of such dyes lies in the catalyst's efficiency, which is related to the nanoparticle stability and surface area of the nanoparticles. However, in large-scale treatment of wastewater, major regulation without altering the pH can be a challenging task for the researchers.

The present-day focus on the green synthesis of metal oxide nanoparticles rather than the conventional methods has been preferred in endorsing the degradation of more toxic compounds to fewer toxic compounds or directly to O_2, CO_2,

✉ Saikatendu Deb Roy
saikatendudebroy7@gmail.com

1 Department of Chemistry, NIT Silchar, Silchar, Assam, India 788010

2 Department of Chemistry, Gurucharan College, Silchar, Assam, India 788004

3 Department of Statistics, Assam University, Silchar, Assam, India 788011

4 Department of Statistics, Gurucharan College, Silchar, Assam, India 788004

and H_2O as by-products along with secondary products. The individual contribution of metal oxide nanoparticles, viz., SrO, CuO, or MnO, are known [20–22]. However, the synthesis of in situ triple-mixed nanoparticles has been a turnabout factor in catalytic application in bioremediation.

The present work includes the synthesis of mixed metal nano-oxide composite of strontium, copper, and manganese using *Carica papaya* fruit extract. The work aims to exploit the efficiency of the nanocomposite in the degradation of both aniline blue (AB) and malachite green (MG) under sunlight as the source of UV in the presence of H_2O_2. The photocatalysts were characterized using scanning electron microscopy (SEM), transmission electron microscopy (TEM), X-ray diffraction (XRD), and energy dispersive spectra (EDS). The degradation of dyes at regular time intervals is studied using a UV spectrometer. The particle size was measured using Debye–Scherrer equation, and Willamson–Hall analysis is performed with XRD data to explore the lattice strain of the material. Lattice strain is present due to imperfection in crystals, which includes lattice dislocation, grain boundary triple junction, contact or sinter stress, coherency stress, etc. Mechanical alloying also contributes to the introduction of strain in powdered samples. X-ray profile analysis is a convenient tool to estimate the crystal strain. [23–26] The statistical analysis on degradation of AB- and MG- data is done. We observed the normality criteria for each variable which is present in AB- and MG- data. To match the requirements of normality, two nonparametric tests, viz., Kolmogorov–Smirnov and Shapiro–Wilk tests, are employed. Kolmogorov–Smirnov test is used to find whether any data has been drawn from a particular probability distribution. Similarly, the Shapiro–Wilk test is also used to check whether any data comes from a normal distribution or not. The objective of the work is to get the degradation time of both aniline blue and malachite green. Multiple linear regression is implemented for getting the degradation time when absorption becomes zero.

2 Experimental

2.1 Materials and method

Strontium nitrate ($Sr(NO_3)_2$) was purchased from Qualigens and cupric sulfate ($CuSO_4$) and potassium permanganate ($KMnO_4$) was purchased from Fisher Scientific, and the chemicals were used without any purification.

2.2 Synthesis of Sr/Cu/MnO composite

SrO/CuO/MnO nanocomposites were prepared via previously reported synthetic procedures reported earlier [11]. Stock solutions of desired concentrations of strontium nitrate, cupric sulfate, and potassium permanganate were prepared. Fresh papaya (*Carica papaya*) was obtained from the local market, and the skin and seeds were removed and boiled for 3 h with the addition of batches of distilled water. The content is then filtered, and the extract is used to prepare the nanocomposite. Fifty milliliters of each stock solution was mixed in a beaker and stirred vigorously with a magnetic stirrer, followed by adding papaya extract in drops. A color change in the solution is noted, and the system is kept in motion for the next 2 h. The solution mixture is then allowed to settle, and a layer of the precipitate is obtained, which is then washed thoroughly with distilled water, followed by drying and then calcination at 520 °C. On removal, the fine powder is crushed with a mortar and pestle.

2.3 Experimental procedures

A 250 ml Erlenmeyer flask was used for the batch experiments. Fifty milliliters of each 30 ppm MG and AB was taken in four separate flasks. During the first set of experiments, in two flasks containing MG and AB, 1 ml of 10% H_2O_2 was added, followed by 30 mg Sr/Cu/MnO composite, and kept in sunlight for degradation. The initial concentration of both MG and AB were recorded, and the samples were taken out from the conical flask periodically and were analyzed immediately. During the experimental proceedings, no alteration in pH was made and performed at room temperature.

2.4 Analytical methods

The efficiency of the experimental processes was evaluated by monitoring the degradation of MG and AB using a double-beam UV/Vis spectrophotometer (Shimadzu, Model UV Japan). The decrease in the absorbance values of MG and AB after irradiation at a particular time shows the efficiency of the nanocomposite photocatalysts and the activity of the material. The degradation efficiency ($D\%$) was calculated as

$$D(\%) = \left(\left(C_0 - C_t\right) \times 100\%\right)\%/C_0 \quad (1)$$

where C_0 and C_t are the concentrations of MG and AB at time 0 (min) and t (min), respectively, and t(min) is the irradiation time.

2.5 Statistical analysis of degradation

Two hypotheses viz., null hypothesis, which considers degradation time is normally distributed, and alternative hypothesis, considering degradation time is not normally distributed. To find the degradation time of the absorption in the case of both AB and MG, multiple linear regression method is used. Multiple regression is a statistical technique and one of the machine learning

tools employed to analyze the interrelation between a single dependent variable and several independent variables. The primary need for multiple regression analysis is to predict the value of a single dependent variable using independent variables whose values are known. In both cases, degradation time in a minute is taken as dependent variable, while considering absorption data of AB and MG is usually distributed. First quartile (x_1), median (x_2), and third quartile (x_3) are selected as three independent variables. The multiple regression model for aniline blue (AB) and malachite green (MG) is provided by Eq. (2) below:

$$y = a + bx_1 + cx_2 + dx_3 \tag{2}$$

y = degradation time in minute;
x_1 = first quartile value of absorption;
x_2 = median value of absorption;
x_3 = third quartile value of absorption.

3 Results and discussion

3.1 Textural characterization of the materials

3.1.1 XRD analysis

The XRD pattern of the nanocomposite is shown in Fig. 1. The polycrystalline nature of the particles has been revealed, and the presence of strontium oxide (SrO) has been observed at 28.6 and 45.23, having planes (101) and (112), complying with JCPDS data no. 820915. Major peak position at 30.1 having plane (311) is due to copper manganese oxide (CuMnO). Other peaks at 32.69, 33.5, 37.7, 54.38, and 62.84 having planes of (110), (200), (005), (020), and (113) is due to the presence of CuO in the sample, complying with JCPDS card no. 481548. The shift in the major peak position may be due to the presence of sulfur and other free metals as an impurity. The intense peaks at 27.0, 42.07, and 44.29 is due to the formation of composite. The major constituent of the composite mixture is SrO, as the intensity of SrO peak is higher as compared to CuO and MnO present in the sample. The other peaks in the spectrum is due to the formation $SrSO_4$ formed due to the sulphate ions from $CuSO_4$ solution. The EDS spectra discussed later are in agreement with the fact that SrO-$SrSO_4$ is the major constituent in the sample. The sharp peaks in the spectra confirm the crystalline nature of the material. The average particle was calculated using Debye–Scherrer's formula:

$$D = 0.89\lambda/(\beta\cos\theta) \tag{3}$$

where D is the crystallite size in nanometer, λ is the wavelength (1.5418 Å), and B is the full width at half maximum. The crystallite size is found to be 20.56 nm.

The total broadening is given by

$$B_T = \beta_D + \beta_\varepsilon \tag{4}$$

where β_D is the broadening due to crystallite size and β_ε is the broadening due to strain.

Peak broadening due to micro-strain is given by

$$\beta_\varepsilon = 4\varepsilon\tan\theta \tag{5}$$

Now rearranging the above equation, we get, and putting the values of Eqs. (3) and (5) in Eq. 4, we get

$$B_T\cos\theta = 4\varepsilon\sin\theta + (K\lambda)/D \tag{6}$$

where $K = 0.89$.

The above equation represents a straight line.

$$y = mx + c \tag{7}$$

where slope m is equal to ε, and from the Willamson–Hall plot, the slope will provide the strain of the material (Fig. 2). For plotting the Willamson–Hall plot, we employ data enlisted in Table 1.

From the above Willamson–Hall plots, the slope ε is found to be 0.42711, which is the strain of the material.

3.1.2 SEM analysis

The Scanning electronic microscopic (SEM) image of Sr/Cu/MnO (Fig. 3a–d) composite as synthesized represents a clear oval texture, and the primary occupancy of SrO-$SrSO_4$ decorated with the presence of MnO and CuO can be visualized easily from the images supported by EDS data. The SEM images in Fig. 3 reveal the fine particle nature of Sr/Cu/MnO in a mixture. All the particles maintained an oval shape, as is worth noting from the overall image of the composite. The particles are fine and aggregated, and the surface of the oval oxides is decorated with other ornamental oxides (Fig. 3b and c) validated from EDS spectra. The fractures in the SEM images are due to surface modification due to

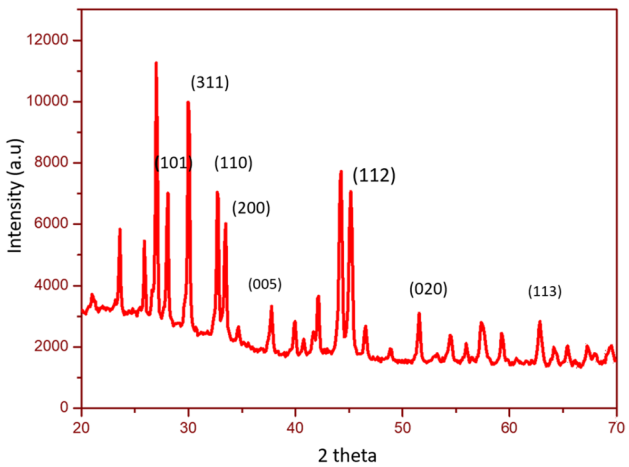

Fig. 1 XRD diffractogram of Sr/Cu/MnO composite

the presence of other oxides together forming the composite material of Sr/Cu/MnO mixed oxides. Figure 3(d) represents the oval surface, which turns out to be rough rather than polished due to the presence of other oxides on the surface of the nano-oxide.

3.1.3 TEM-EDS analysis

The morphology and particle size of Sr/Cu/MnO are studied using TEM (Fig. 4(a–d)). The TEM images of the prepared Sr/Cu/MnO nanocomposite and Fig. 4(e), representing the histogram, reveals the average particle size is 83 nm. The particles are agglomerated, and the surface of the corresponding material reveals the surface decoration with spherical agglomerates. Similarities in the spherical structure can be easily observed from SEM and TEM images. The particle size calculated by the Debye–Scherrer equation finds relevance from the histogram, where the highest bar is observed nearly at 25 nm length.

The EDS reveals the elemental composition of the sample (Fig. 5). The spectral data clearly represents the presence of Sr, Cu, Mn, and O as the constituent. The appearance of sharp

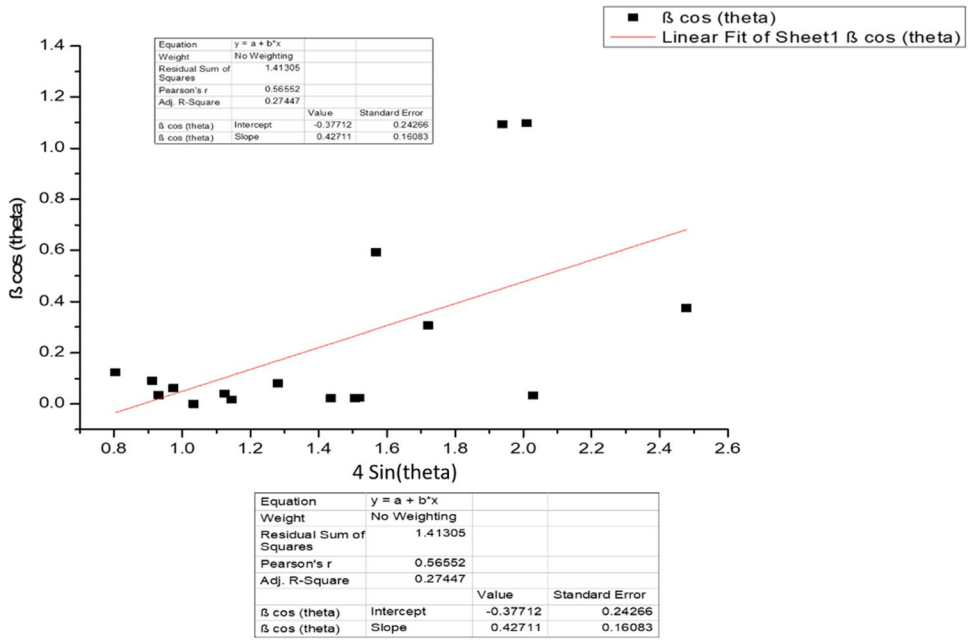

Fig. 2 Willamson–Hall plot indicating the line broadening due to strain

Table 1 Peak indexing and values of FWHM to plot Willamson–Hall plot

Peak position 2θ (°)	θ (radians)	FWHM (degree)	FWHM (radian)	$\beta \cos\theta$	4 $\sin\theta$
23.18871	0.202359669	7.26287	0.126760995	0.124174444	0.803925635
26.34702	0.229921124	5.33914	0.093185572	0.090733336	0.911602894
26.91851	0.234908315	2.05428	0.03585395	0.034869246	0.931015277
28.19268	0.246027545	3.67299	0.064105769	0.062175389	0.974212227
29.93718	0.26125118	0.02158	0.000376642	0.000363862	1.033157912
32.66709	0.285074139	2.37451	0.041443018	0.039770411	1.124914395
33.28176	0.290438146	1.03759	0.018109362	0.017350914	1.145488195
37.3416	0.325866934	4.90491	0.085606829	0.081101646	1.280520866
42.07836	0.367202963	1.36459	0.023816588	0.022228859	1.436025067
44.24266	0.386090043	1.34776	0.02352285	0.021791297	1.506276656
46.16602	0.402874526	36.9232	0.64443141	0.592836812	1.568257373
44.66794	0.389801312	1.50328	0.026237186	0.024268992	1.520018555
50.96594	0.44476173	19.43555	0.339214339	0.306213264	1.720971211
57.95928	0.505790134	71.58277	1.249355024	1.092925691	1.937995177
60.35373	0.526685652	72.81131	1.270797092	1.098575928	2.010683708
60.97698	0.532124534	2.17794	0.038012224	0.032756316	2.029461049

peak near strontium is due to the sulfur from $CuSO_4$ solution resulting to formation of $SrSO_4$ with the composite using *Carica papaya* fruit extract. The major constituent of the material is oxygen, present in the form of oxides with other elements. The spectral data is in agreement with the fact that the nanocomposite contains Sr/Cu/MnO as its primary constituent.

3.2 Particle crystallinity index

Peak breath and specific phases are proportional to the crystallinity index of the material. The sharper the XRD, the larger the crystalline peaks. The particle size calculated from the Debye–Scherrer equation is 20.56 nm. The particle's crystallinity is evaluated by comparing the particle size obtained from the Scherrer equation and those calculated from the TEM image. The crystallinity equation is represented as

$$I_{cry} = D_{\mathrm{p}}(\text{TEM or SEM})/D(\text{XRD}) \tag{8}$$

where I_{cry} is the crystallinity index, D_{p} is the particle size from TEM images, and D is the particle size calculated from XRD data using Debye–Scherrer equation. [27] The particle crystallinity is summarized in Table 2.

3.3 Photocatalytic degradation

Representation for the photocatalytic degradation of two commercial dyes, viz., aniline blue (AB) and malachite green (MG), has been represented above. The uniform decrease in the absorbance of both aniline blue (AB) and malachite green (MG) has been achieved without altering the pH of the medium. Aniline blue (AB) and malachite green (MG) absorb at wavelengths 599 and 617 nm, respectively. The degradation efficiency of the photocatalyst was calculated using Eq. (1), as mentioned earlier. The percentage of degradation of AB turns out to be 74.21% and that of MG is 91.07% in the span of 150 min (Fig. 6).

A statistical tool has been used to calculate the probable time for the complete degradation of both dyes. To check the normality at different degradation times of aniline blue and malachite green, two nonparametric tests were used, namely Kolmogorov–Smirnov and Shapiro–Wilk. Both Kolmogorov–Smirnov and Shapiro–Wilk tests reject the null hypothesis that the data is normally distributed since the *p*-value is less than 0.05 at a 5% significance level. The same is summarized in Tables 3 and 4. It is observed that data is not uniform in nature. Thus, transforming data into a normal one by using the df (data transformation), or normal function under inverse df (data transformation) in SPSS. The data transformation is a tool used for changing non-normal data into normal one. After transforming aniline blue and malachite green for different degradation times, again normality test is performed on transformed data. It is found that data is normally distributed since the *p*-value is greater than 0.05 at a 5% significance level (Tables 5 and 6). Descriptive analysis of both aniline blue and malachite green is provided in Tables 7 and 8. The number of responses recorded in each

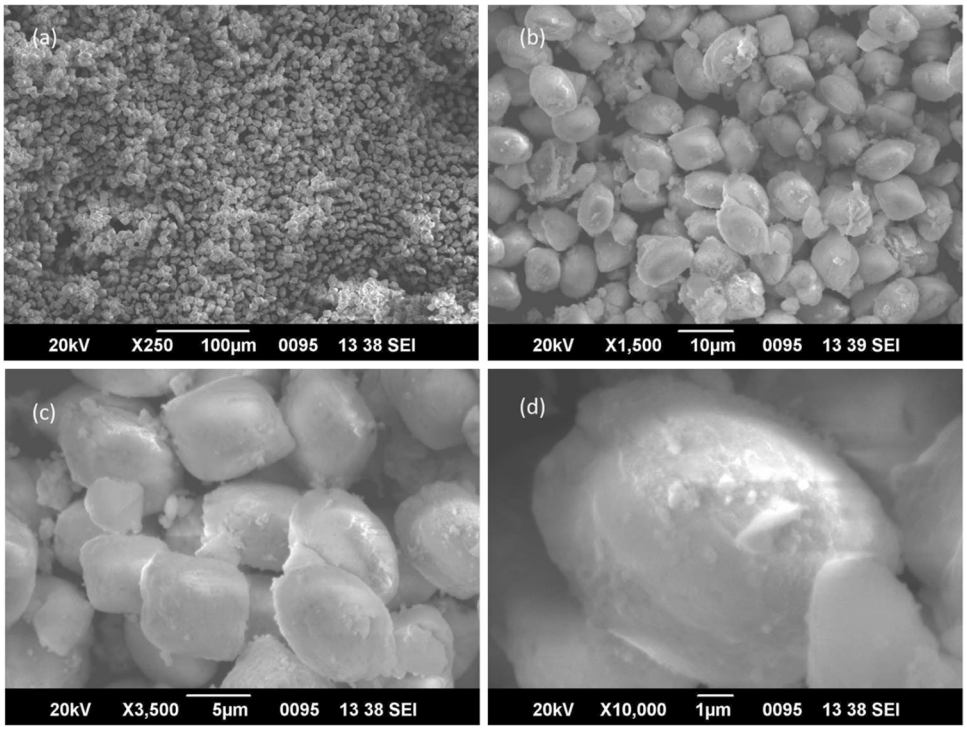

Fig. 3 SEM image of the synthesized nanocomposite representing the distinct spherical structure (**a**–**d**)

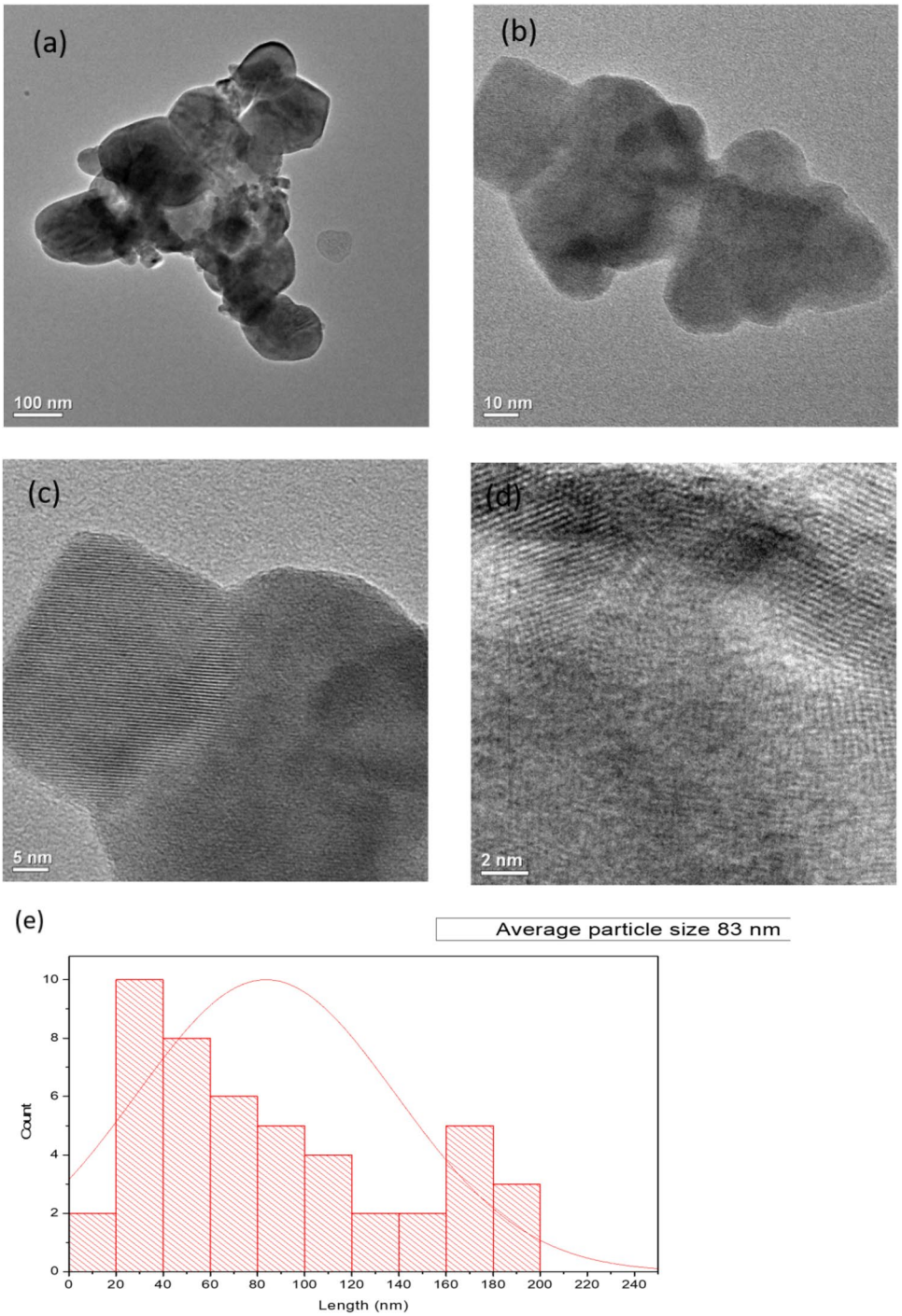

Fig. 4 TEM images of the Sr/Cu/MnO nanocomposite (**a**–**d**) and histogram of average particle size (**e**) calculated from TEM

degradation time with absorption is 803. The degradation time is provided in minutes, and it starts from 0, 10, 20, and lastly, it goes up to 150 with their absorption value. The value of the first quartile, median, and third quartile were provided for each degradation time since the first quartile contains 25% of the entire dataset. Similarly, the median and third quartiles contain 50 and 75% of the whole dataset. Using this information and applying machine learning algorithm we computed absorption time for both aniline blue and malachite green.

To find the exact time when the concentration of aniline blue (AB) becomes zero, the entire data is transformed into a normal distribution. The equidistant values first quartile is computed with median and third quartile. Using these three independent variables and degradation time in a minute as a dependent

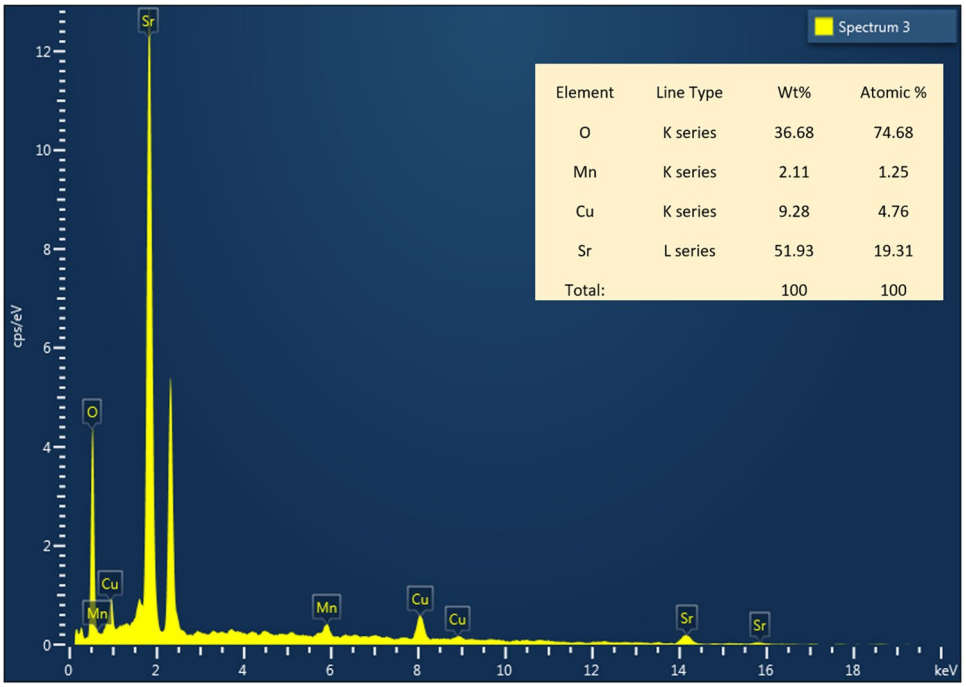

Fig. 5 EDS spectrum of the nanocomposite

Table 2 Crystallinity index of the nanocomposite

Sample	D_p (nm)	D (nm)	I_{cry} (unitless)	Particle type
SrO/CuO/MnO	83	20.56	4.036	Polycrystalline

variable, multiple regression model is fitted, which is represented in Eq. (2). The multiple regression model is a good fit with a R^2 value of 98.42 and adjusted R^2 97.63. The regression analysis result of aniline blue are summarized in Table 9. The independent variables turned out to be significant, with a p-value of more than 0.05. Thus, to get the degradation time in minutes when the absorption will become zero (0), all the independent variables is assumed to be 0, which indicates a flat line of the absorption around the x-axis. After executing the regression models, finally, the degradation time around 184.2 min is observed, which can be approximated to 180 min. Thus, after 3 h, the absorption will become zero (0) in the case of aniline blue (AB). However, Table 10 represents the multiple regression model for malachite green (MG), which fits well with a R^2 value of 97.01 and adjusted to R^2 of 96.01. On parallel execution, after calculating the degradation time it is found to be 152.2 min, which is approximated as 152 min, thus, after 152 min, the absorption will become zero (0) in the case of malachite green (MG).

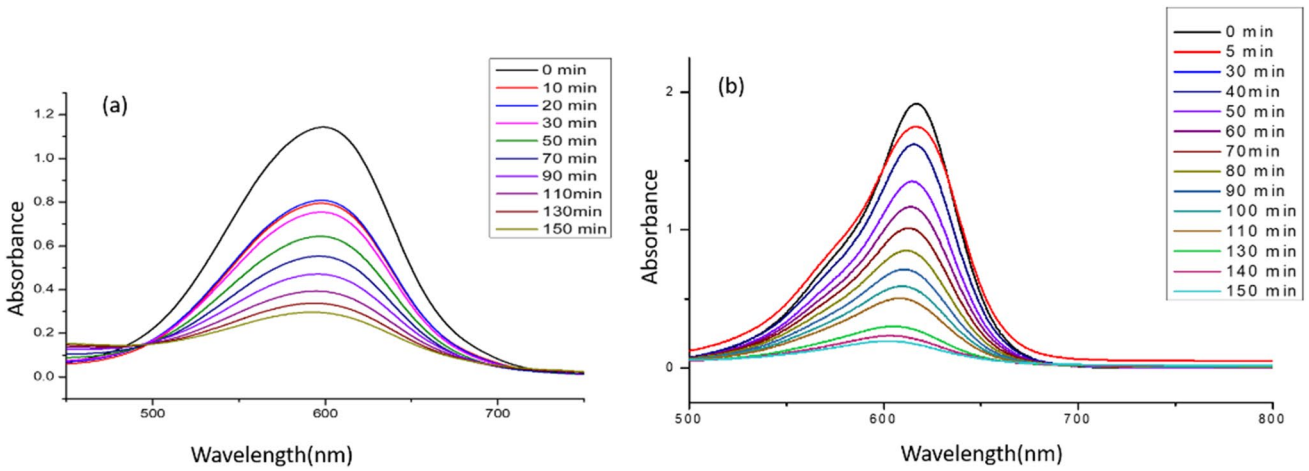

Fig. 6 **a** Photocatalytic degradation of aniline blue; **b** photocatalytic degradation of malachite green

Table 3 Test of normality on raw aniline blue (AB)

Degradation time (min)	*P*-value	
	Kolmogorov–Smirnov[a]	Shapiro–Wilk
0	0.000	0.000
10	0.000	0.000
20	0.000	0.000
30	0.000	0.000
50	0.000	0.000
70	0.000	0.000
90	0.000	0.000
110	0.000	0.000
130	0.000	0.000
150	0.000	0.000

Table 4 Test of normality on raw malachite green (MG)

Degradation time (min)	*P*-value	
	Kolmogorov–Smirnov[a]	Shapiro–Wilk
0	0.000	0.000
5	0.000	0.000
30	0.000	0.000
40	0.000	0.000
50	0.000	0.000
60	0.000	0.000
70	0.000	0.000
80	0.000	0.000
90	0.000	0.000
100	0.000	0.000
130	0.000	0.000
150	0.000	0.000

Table 5 Test of normality on transformed aniline blue (AB)

Degradation time (min)	*P*-value	
	Kolmogorov–Smirnov[a]	Shapiro–Wilk
0	0.200	0.086
10	0.200	0.064
20	0.200	0.132
30	0.200	0.014
50	0.200	0.046
70	0.200	0.042
90	0.029	0.085
110	0.200	0.190
130	0.200	0.029
150	0.138	0.024

Table 6 Test of normality on modified malachite green (MG)

Degradation time (min)	*P*-value	
	Kolmogorov–Smirnov[a]	Shapiro–Wilk
0	0.200	0.083
5	0.200	0.035
30	0.155	0.085
40	0.175	0.034
50	0.200	0.087
60	0.205	0.045
70	0.200	0.078
80	0.210	0.078
90	0.215	0.104
100	0.197	0.046
130	0.267	0.143
150	0.245	0.137

Table 7 Descriptive analysis on modified aniline blue (AB)

Degradation time (min)	*No. of observations*	*Absorption*		
		First quartile	*Median*	*Third quartile*
0	803	0.10	0.36	0.62
10	803	0.08	0.26	0.44
20	803	0.08	0.26	0.44
30	803	0.08	0.25	0.42
50	803	0.08	0.22	0.36
70	803	0.08	0.2	0.32
90	803	0.09	0.19	0.29
110	803	0.09	0.17	0.25
130	803	0.09	0.16	0.23
150	803	0.09	0.15	0.21

Table 8 Descriptive statistics on modified malachite green (MG)

Degradation time (min)	No. of observations	Absorption		
		First quartile	Median	Third quartile
0	801	0.023	0.380	0.730
5	801	0.090	0.420	0.750
30	801	0.035	0.340	0.640
40	801	0.035	0.290	0.540
50	801	0.030	0.260	0.480
60	801	0.040	0.230	0.420
70	801	0.040	0.200	0.360
80	801	0.040	0.170	0.310
90	801	0.040	0.150	0.260
100	801	0.040	0.130	0.230
130	801	0.040	0.090	0.150
150	801	0.040	0.080	0.130

Table 9 Regression analysis table of aniline blue (AB)

	Estimate	*T*-value	*P*-value
Intercept	184.2	1.595	0.1618
x_1	− 721.7	− 1.767	0.1276
x_2	2801.6	1.832	0.1166
x_3	− 1912.1	− 2.683	0.0364
R^2= 98.42		Adj. R^2= 97.63	

Table 10 Regression analysis table of malachite green (MG)

	Estimate	*T*-value	*P*-value
Intercept	152.2	17.797	2.53 e^{-08}
x_1	− 307.744	− 0.731	0.484
x_2	1104.408	1.231	0.250
x_3	− 779.873	− 1.705	0.122
R^2= 97.01		Adj. R^2 = 96.01	

4 Possible mechanism of degradation

Heterogeneous photocatalysis consists of a sequence of reaction events co-occurring. Some reported mechanism includes five-step processes that contains (1) diffusion of reactant to the surface of the material, (2) adsorption on the surface, (3) reaction occurring on the surface, and (4) diffusion of products formed on the surface. [8, 10] The reaction medium includes H_2O_2, which generates OH free radicals. The proposed mechanism can be summarized as

$$\mathrm{Sr/Cu/MnO} + h\nu \rightarrow \mathrm{Sr/Cu/MnO}\left(e_{\mathrm{CB}}^{-}\right) + \mathrm{Sr/Cu/MnO}\left(h_{\mathrm{VB}}^{+}\right)$$

$$\mathrm{Sr/Cu/MnO}\left(h_{\mathrm{VB}}^{+}\right) + \mathrm{H_2O} \rightarrow \mathrm{Sr/Cu/MnO} + \mathrm{OH} + \mathrm{H^+}$$

$$\mathrm{Sr/Cu/MnO}\left(h_{\mathrm{VB}}^{+}\right) + \mathrm{OH^-} \rightarrow \mathrm{Sr/Cu/MnO} + \mathrm{OH}$$

$$\mathrm{Sr/Cu/MnO}\left(e_{\mathrm{CB}}^{-}\right) + \mathrm{O_2} + \mathrm{H^+} \rightarrow \mathrm{Sr/Cu/MnO} + \mathrm{HO_2} \rightarrow \mathrm{O_2^-} + \mathrm{H^+}$$

$$\mathrm{Sr/Cu/MnO}\left(h_{\mathrm{VB}}^{+}\right) + \mathrm{dye} \rightarrow \text{oxidation of dye}$$

$$\mathrm{OH} + \mathrm{dye} \rightarrow \text{degradation of dye}$$

The catalytic efficiency of individual MnO, CuO, or SrO nanoparticles is known. The surface modification with the presence of Sr/CuO/MnO seems to enhance the photocatalytic activity. The surface decoration can result in enhanced effect in photocatalytic activity.

5 Comparison with other works

The present work reported includes mixed metal oxide composite of Sr/Cu/MnO synthesized via co precipitation method. The efficiency of the photocatalyst is seen to be comparable with the other reported catalysts. The data has been summarized in Table 11.

6 Conclusion

Mixed Sr/Cu/MnO nano-oxide has been obtained via co-precipitation method using *Carica papaya* extract. The composite has the efficiency of degrading both malachite green (MG) and aniline blue (AB) in short period of time without acid. The mixed nano-oxide composite has been analyzed using XRD, SEM, TEM, and EDS techniques. The particle size lies in close agreement with the one calculated from the XRD data and TEM histogram diagrams. The Willamson–Hall plot constructed reveals the strain of the material to be 0.42711 and particle crystallinity index is calculated to be 4.036. The degradation of dyes has followed the photo-Fenton-like mechanism with H_2O_2 as an oxidant. It is observed that the catalyst has degraded 74.2% of aniline blue (AB) and 91.07%

Table 11 Comparison of photocatalyst with other reported catalysts

Catalyst	Dye degraded	Amount	Percentage of degradation	Reference
ZnO	Malachite green	0.2 g/l	85.29% in 100 min	[28]
TiO_2	Malachite green	0.6 g/l	95% in 60 min	[29]
MnO_2-MCM	Malachite green	1 g/l	100% in 60 min	[30]
Ag_2O.SrO.CaO	Methylene violet	0.03–0.07 g/l	100% at 0.05 conc in 120 min	[31]
Fe_3O_4-PDA betonite	Rhodamine blue and crystal violet		93% in 60 min	[32]
ZnO/SrO composite	Methylene blue		96.5% in 60 min	[33]
Sr/Cu/MnO	Aniline blue and malachite green	30 mg in 50 ml	Aniline blue 74.21% and malachite green 91.07% in 150 min	This work

of malachite green (MG) dye, which are used on an industrial scale. The statistical approach has revealed that the complete degradation of both aniline blue (AB) and malachite green (MG) can be achieved at 180 and 152 min, respectively. From the results, it can be concluded that material is promising and can be categorized as one of the efficient nanocatalysts reported.

Acknowledgements Authors are thankful to Dr. Abhijit Nath, Department of Chemistry GC College, for his constant support, suggestion, and encouragement during the experimental proceedings. Authors also greatly acknowledge the support of the Department of Chemistry at NIT Silchar, SAIF NEHU (Shillong) for SEM and TEM images, the Central Instrumentation Facility at NIT Silchar for XRD analysis, and STIC Cochin University for SEM EDAX analysis.

Author contribution Saikatendu Deb Roy: Experimentation, data analysis, and preparation of manuscript. Bireswar Bhattacherjee: Sataistical analysis. Krishna C Das: Editing. Siddhartha S Dhar: Overall supervision.

Data availability Data will be made available on request.

Declarations

Ethical approval Not applicable since the study was not carried out with any animal models.

Competing interests The authors declare no competing interests.

References

1. Basavarajappa PS, Seethya NHB, Ganganagappa N, Eshwaraswamy KB, Reddy KR, (2018) Enhanced photocatalytic activity and biosensing of gadolinium substituted BiFeO 3 nanoparticles. 9025–9033. https://doi.org/10.1002/slct.201801198
2. Khataee AR, Mirzajani O (2010) UV/peroxydisulfate oxidation of C.I. Basic blue 3: modeling of key factors by artificial neural network. Desalination 251:64–69
3. Daneshvar N, Aber S, Vatanpour V, Rasoulifard MH (2008) Electro-Fenton treatment of dye solution containing orange II: influence of operational parameters. J Electroanal Chem 615:165–174
4. Saha S, Wang JM, Pal A (2012) Nano silver impregnation on commercial TiO2 and a comparative photocatalytic account to degrade malachite green. Sep Purif Technol 89:35–44
5. Rao A, Sivasankar BN, Sadasivam V (2010) Comparative studies on photocatalytic efficiency of ZnO and TiO2 for decolonization and mineralization of orange II. Pollut Res 29:613–619
6. Rao A, Sivasankar BN, Sadasivam V (2010) Photo-oxidative degradation of an azo dye direct red 31 in the presence of ZnS catalyst. Indian J Chem A 49:901–905
7. Hameeda BH, El-Khaiary MI (2008) Malachite green adsorption by rattan sawdust: isotherm, kinetic and mechanism modeling. J Hazard Mater 159:574–579
8. Rajabi HR, Khani O, Shamsipur M, Vatanpour V (2013) High-performance pure and Fe3+-ion doped ZnS quantum dots as green nanophotocatalysts for the removal of malachite green under UV-light irradiation. J Hazard Mater 250:370–378
9. Khataee AR, Vantanpour V, Amani AR (2009) Decolorization of C.I. Acid blue 9 solution by UV/nano-TiO2, Fenton, Fenton-like, electro-Fenton and electrocoagulation processes: a comparative study. J Hazard Mater 161:1225–1233
10. Pirkanniemi K, Sillanpää M (2002) Heterogeneous water phase catalysis as an environmental application: a review. Chemosphere 48(10):1047–1060
11. Roy SD, Goswami M, Das KC, Dhar SS (2022) Bio-benign synthesis of strontium, copper, and manganese nano-hydroxide from Carica papaya unveiling potential biocidal activity against bacterial strains and conversion to oxides and its characterization. Biomass Convers Biorefinery 1–8
12. Srivastava S, Sinha R, Roy D (2004) Toxicological effects of malachite green. Aquat Toxicol 66:319–329
13. Lee JC, Kim MS, Kim CK, Chung CH, Cho SM, Han GY, Yoon KJ, Kim BW (2003) Removal of paraquat in aqueous suspension of TiO2 in an immersed UV photoreactor. Korean J Chem Eng 20:862–868
14. Fenton HJH (1894) Oxidation of tartaric acid in presence of iron. J Chem Soc 65:899–911
15. Bishop F, Stern G, Fleischman M, Mar Shall LS (1968) Hydrogen peroxide catalytic oxidation of refractory organics in municipal waste waters. Ind Eng Chem Proc Des Dev 7:1110–1117
16. Kuo WG (1992) Decolorizing dye wastewater with Fenton's reagent. Water Res 26:881–886
17. Tang WZ, Huang CP (1996) 2,4-Dichlorophenol oxidation kinetics by Fenton's reagent. Environ Technol 17:1371–1378
18. Barbusinski K, Filipek K (2001) Use of Fenton's reagent for removal of pesticides from ´ industrial wastewater, Polish. J Environ Stud 10:207–212
19. Hameed BH, Lee TW (2009) Degradation of malachite green in aqueous solution by Fenton process. J Hazard Mater 164(2–3):468–472
20. Dang TD, Banerjee AN, Tran QT, Roy S (2016) Fast degradation of dyes in water using manganese-oxide-coated diatomite for environmental remediation. J Phys Chem Solids 98:50–58
21. Singh J, Kumar V, Kim KH, Rawat M (2019) Biogenic synthesis of copper oxide nanoparticles using plant extract and its prodigious potential for photocatalytic degradation of dyes. Environ Res 177:108569
22. Indulal CR, Ravikumar R, Biju R, Akhil M, Suresh K (2019) Optical and photocatalytic studies of zinc strontium oxide nanocomposite for technological applications. In AIP Conference Proceedings (Vol. 2100, No. 1, p. 020057). AIP Publishing LLC
23. Mote VD, Purushotham Y, Dole BN (2012) Williamson-Hall analysis in estimation of lattice strain in nanometer-sized ZnO particles. J Theor Appl Phys 6(1):1–8
24. Ungár T (2007) Characterization of nanocrystalline materials by X-ray line profile analysis. J Mater Sci 42(5):1584–1593
25. Suryanarayana C (2001) Mechanical alloying and milling. Prog Mater Sci 46(1–2):1–184
26. Cullity BD, Stock SR (2001) Elements of x-ray diffraction. Prentice Hall, Upper Saddle River, NJ, p 388
27. Theivasanthi T, Alagar M (2011) Electrolytic synthesis and characterizations of silver nanopowder. arXiv preprint arXiv:1111.0260
28. Navada KK, Kulal A (2020) Enhanced production of laccase from gamma irradiated endophytic fungus: a study on biotransformation kinetics of aniline blue and textile effluent decolourisation. J Environ Chem Eng 8(2):103550
29. Saikia L, Bhuyan D, Saikia M, Malakar B, Dutta D, Sengupta P (2015) Photocatalytic performance of ZnO nanomaterials for self

sensitized degradation of malachite green dye under solar light. Appl Catal Gen 490:42e49. https://doi.org/10.1016/j.apcata.2014.10.053
30. Ma Y, Ni M, Li S (2018) Optimization of malachite green removal from water by TiO2 nanoparticles under UV irradiation. Nanomaterials 8:428. https://doi.org/10.3390/nano8060428
31. Nanda B, Pradhan A, Parida K (2016) A comparative study on adsorption and photocatalytic dye degradation under visible light irradiation by mesoporous MnO2 modified MCM-41 nanocomposite. Microporous Mesoporous Mater 226:229e242. https://doi.org/10.1016/j.micromeso.2015.12.027
32. Subhan MA, Rifat TP, Saha PC, Alam MM, Asiri AM, Rahman MM, ... Uddin J (2020) Enhanced visible light-mediated photocatalysis, antibacterial functions and fabrication of a 3-chlorophenol sensor based on ternary Ag 2 O· SrO· CaO. RSC Adv 10(19):11274–11291
33. Ain QU, Rasheed U, Yaseen M, Zhang H, Tong Z (2020) Superior dye degradation and adsorption capability of polydopamine modified Fe3O4-pillared bentonite composite. J Hazard Mater 397:122758
34. Harish S, Sabarinathan M, Archana J, Navaneethan M, Nisha KD, Ponnusamy S, ... Hayakawa Y (2017) Synthesis of ZnO/SrO nanocomposites for enhanced photocatalytic activity under visible light irradiation. Appl Surf Sci 418:147–155